HHS Public Access

Author manuscript

Nat Photonics. Author manuscript; available in PMC 2013 September 24.

Published in final edited form as:

Nat Photonics. 2013 ; 7: 285–289. doi:10.1038/nphoton.2013.25.

Silicon coupled with plasmon nanocavity generates bright visible hot-luminescence

Chang-Hee Cho[†,‡], **Carlos O. Aspetti**[‡], **Joohee Park**, and **Ritesh Agarwal**[*]

Department of Materials Science and Engineering, University of Pennsylvania, Philadelphia, Pennsylvania 19104, USA

Abstract

Due to limitations in device speed and performance of silicon-based electronics, silicon optoelectronics has been extensively studied to achieve ultrafast optical-data processing[1–3]. However, the biggest challenge has been to develop an efficient silicon-based light source since indirect band-gap of silicon gives rise to extremely low emission efficiency. Although light emission in quantum-confined silicon at sub-10 nm lengthscales has been demonstrated[4–7], there are difficulties in integrating quantum structures with conventional electronics[8,9]. It is desirable to develop new concepts to obtain emission from silicon at lengthscales compatible with current electronic devices (20-100 nm), which therefore do not utilize quantum-confinement effects. Here, we demonstrate an entirely new method to achieve bright visible light emission in “bulk-sized” silicon coupled with plasmon nanocavities from non-thermalized carrier recombination. Highly enhanced emission quantum efficiency (>1%) in plasmonic silicon, along with its size compatibility with present silicon electronics, provides new avenues for developing monolithically integrated light-sources on conventional microchips.

In bulk silicon, emission from hot-carriers (non-thermalized carrier recombination) has been observed by injecting carriers at large applied bias[10]; however, the measured quantum efficiency is extremely low because hot-carrier relaxation time (intra-band; 0.1–1 ps) is much faster than radiative lifetime (∼10 ns)[11–14], leading to very poor efficiency ($<10^{-4}$) for hot-luminescence across the direct band at the Γ point. However, visible light emission from hot-carriers in “bulk” silicon can be efficient if the radiative lifetime becomes comparable with the hot-carrier relaxation time. In addition, enhanced emission from hot-carriers in silicon can enable studies of photophysics of indirect bandgap materials, which is otherwise challenging due to intrinsic low-emission quantum yields. Although silicon photonic crystal nanocavities have recently demonstrated Purcell enhancements up to 100, the emission was

[*]To whom correspondence should be addressed. riteshag@seas.upenn.edu.

[†]Present address: Department of Emerging Materials Science, Daegu Gyeongbuk Institute of Science & Technology (DGIST), Daegu 711-873, Korea

[‡]These authors contributed equally to this work.

Author contributions: C-H. C. and R. A. developed the concept and design of the devices. C-H. C. fabricated the devices and performed optical measurements. C. O. A. performed the numerical simulations, fabricated devices and performed optical measurements at 532 nm excitation. J. P. fabricated and carried out the emission experiments on bowtie structures. C-H. C., C. O. A. and R. A. analyzed the results and wrote the manuscript.

mostly generated from thermalized carriers in the near-infrared wavelength range.[15,16]. Here, we demonstrate visible light emission with high quantum yield (>1%) at room temperature from “bulk-sized” (no quantum-confinement) silicon integrated with a plasmonic nanocavity via the Purcell enhancement effect[17,18,]. Highly concentrated electromagnetic fields inside plasmon nanocavities induce phonon-assisted light emission from hot-carriers before their thermalization to the lowest energy state (near X-point) in the conduction band (Fig. 1a). The interaction of charged carriers with phonons and size-tunable nanocavity plasmons presents new ways to modulate the emission efficiency in silicon devices in the visible range.

To generate light emission from hot-carriers, we fabricated the plasmonic nanocavity on single silicon nanowires (30–80 nm diameter range) by depositing a 5 nm SiO_2 interlayer (to prevent recombination of carriers at the metal surface while maintaining strong nanocavity plasmon fields in silicon), followed by a 100 nm-thick silver Ω-shaped cavity (see Methods) to support surface plasmon polariton modes (Figs. 1b to 1d). Room temperature micro-photoluminescence measurements were carried out on individual nanowire devices with an Ar^+ laser excitation source (2.708 eV). Bright visible light emission was observed from single-plasmonic silicon nanowires (Fig. 1e). Since hot-carrier emission competes with intra-band relaxation, a broad hot-luminescence band is expected ranging from the laser excitation to the indirect band-gap energy in silicon. Figure 1f shows broad hot-luminescence spectra with high counts obtained from a single silicon nanowire coupled with Ω-shaped cavity (Si diameter, d = 65 nm), while no observable photon counts were detected from 5 nm SiO_2 coated silicon nanowires (d = 60 nm) without the silver nanocavity (nanowire lengths are typically 10 μm). Furthermore, under UV laser excitation at 3.486 eV, the hot-luminescence band was observed to extend to the laser excitation energy, resulting in a broad UV to visible light emission (Supplementary Fig. S1). These observations suggest that the hot-carriers emit photons through a phonon-assisted recombination process during intra-band relaxation. Furthermore, in order to test the generality of visible hot-luminescence in plasmonically-coupled silicon, we performed experiments on planar silicon patterned with Ag-bowtie structures (Supplementary Fig. S2), confirming a similar spectrum as that of plasmonic Si nanowires with hot-luminescence bands.

To study the effect of size-tunable plasmonic nanocavity resonances on hot-luminescence, various-sized silicon nanowires (d, 30 to 80 nm) coupled with Ω-shaped cavity were examined. We found that the intensity of the hot-luminescence band (integrated counts) reached a maximum at a resonant size (d = 70 nm), with a clear peak structure reflecting phonon-assisted hot-luminescence processes (Fig 2a). To study the corresponding electromagnetic field distribution and the nanocavity Purcell enhancement, numerical simulations were performed for the Ω-shaped devices (see Methods). The simulated frequency-dependent electromagnetic field intensity inside the cavity (d = 70 nm) correctly reproduces the resonance peaks observed in the hot-luminescence spectrum (Fig. 2a). However, the observed photoluminescence spectrum shows more structure, which is related to the complex phonon-related carrier relaxation channels (peaks 1 to 5 in Fig. 3a, discussed later). Simulations further reveal a plasmonic cavity mode along the Ag/SiO_2 interface perpendicular to the nanowire's long axis, as shown in Figs. 2b-d. Waveguide modes

propagating along the long-axis cannot be supported in the plasmonic nanowires because of the high propagation losses (10 to 30 dB/μm)[17], which have been confirmed by three-dimensional simulations (Supplementary Fig. S4). For the highly-confined plasmonic cavity modes, the quality factor was estimated to be ~30 along with an ultrasmall mode volume of $\lambda^3/10^4$ (λ, free-space wavelength), giving rise to a large radiative rate enhancement (Purcell factor $>10^3$) at 2.505 eV (see Methods). The position-dependent Purcell factor map shows an enhancement of $\sim 10^3$ (<5 nm from the Si surface) and $>10^2$ enhancement throughout the majority of the nanowire core (Supplementary Fig. S5). Note that the actual emission rate is also related to the frequency matching between the cavity resonance and the homogeneously broadened emitter frequencies[19–21]. To estimate the spontaneous emission rate enhancement from the Purcell factors, we calculated the enhanced rates as a function of energy mismatch between the emitter and cavity modes, for both resonant (d = 70 nm) and non-resonant (d = 50 nm) sized nanowires, and obtained spontaneous emission enhancement of $>10^3$ for the resonant size (d = 70 nm) near the nanowire surface (Supplementary Fig. S6). The spectral out-coupling efficiency, which resembles the spectral shape of the cavity field intensity, further modulates the emission intensity of hot-luminescence (Supplementary Fig. S7), resulting in an order of magnitude higher photon counts for the resonant case (see Supplementary information for a detailed discussion). Such large enhancement enables hot-carrier recombination before their thermalization (Fig. 1a), which would otherwise lead to poor radiative quantum yields ($<10^{-4}$). Internal quantum efficiency for hot-luminescence in plasmonic silicon was estimated to be 1.4% (see Methods), with an enhancement of $>10^3$ in comparison to bulk silicon, which can be further improved by optimizing the plasmonic cavity structure.

To understand the interplay of silicon phonon modes and nanocavity plasmon resonances leading to efficient light emission, we carried out polarization-dependent photoluminescence measurements. Since surface plasmon polaritons are transverse-magnetic waves at the metal-dielectric interface[22], the electric-field of plasmon cavity modes should be polarized perpendicular to the nanowire long axis. Indeed, the resonant-sized plasmon cavity (d = 70 nm) showed perpendicularly-polarized hot-luminescence bands with the emission polarization ratio, ρ, of 0.56 where $\rho = (I_\perp - I_{/\!/})/(I_\perp + I_{/\!/})$ (Fig. 3a). The polarized emission bands are exactly overlapped with the calculated field intensity inside the cavity (Fig. 3a); however, the finer peak structures observed within the cavity resonances are more pronounced for the perpendicularly-polarized emission and cannot be simulated by the field calculations. On the other hand, for the non–resonant case (for sizes showing low photon counts), distinct bands attributed to cavity plasmons and phonon-assisted hot-carrier emission were observed. Perpendicularly-polarized hot-luminescence spectra (Figure 3b) along with the calculated cavity field intensity for a nonresonant plasmonic nanowire (d = 50 nm) reveals both the cavity modes and the phonon-assisted luminescence bands, while the parallel polarization shows very little counts. The simulated frequency-dependent cavity field intensity fits reasonably well with the observed modes; interestingly, the sharp peaks assigned to phonon-assisted hot-luminescence bands (“P”) occur at almost the same energies as resonant-sized cavities, but their mismatch with the cavity plasmon bands (“C”) makes the emission process less likely. Even though the “C” modes are off-resonance from the highly emissive hot-carrier states (“P”) in the nonresonant case, the cavity modes can

interact with hot-carrier states with lower density of states and emit, albeit with low counts. To ensure that the sharp peaks originate from the phonon-assisted hot-luminescence bands, we measured spectra at different laser excitation energy (2.331 eV), confirming that the shift of peak ("P") positions (from the laser line) and the interplay between the "P" and "C" peaks (Supplementary Fig. S8).

Our finding is that the phonon-assisted hot-luminescence is greatly enhanced when the hot-carriers assisted by phonons with the highest density of states are resonantly coupled with the cavity plasmons. The simulated size dependence of plasmon cavity modes (Fig. 3c) shows that the exact resonance between the three strong hot-luminescence bands observed at 2.51, 2.34, and 2.18 eV and the plasmon cavity modes occurs at the Si nanowire size of ∼70 nm. This simulated prediction is further verified from the size-dependent photoluminescence spectra of nanowires with diameters ranging from 40 to 80 nm (Fig. 3d). As the diameter approaches the resonant size of ∼70 nm, the hot-luminescence intensity is drastically increased, reflecting a perfect resonance between the hot-carriers assisted by high-density of states phonons and the cavity plasmons. Additionally, there is another predicted resonance (at ∼55 nm) between high-density phonons and cavity modes, which is also measured experimentally.

It should be noted that light emission is only possible when phonons scatter the hot-carriers to the almost vertical light-line ($k \sim 0$). This phonon-assisted scattering process should satisfy momentum conservation, $k' = k_e \pm q \approx 0$, where k' and k_e are the momentum values of hot-carriers at the light line and at the initial electronic state respectively, and q is the phonon momentum. Thus, the hot-carrier population would depend on the phonon modes with the highest density of states where phonon dispersion has almost zero slope[23], where those specific phonons can scatter the hot-carrier efficiently to the light-line. The phonon dispersion of silicon along the <110> direction shows that the density of states is relatively high for momentum values of $\sim 2\pi/a(0.6, 0.6, 0)$ for transverse optical (TO) and transverse acoustic (TA) and $\sim 2\pi/a(0.7, 0.7, 0)$ for longitudinal optical (LO) and TA phonons, situated between Γ and K points[24] (Supplementary Fig. S9a). Taking into account the electronic dispersion of silicon[25] (Supplementary Fig. S9b), the same momentum values of $\sim 2\pi/a(0.6, 0.6, 0)$ and $\sim 2\pi/a(0.7, 0.7, 0)$ correspond to the strong hot-luminescence bands at 2.51 and 2.18 eV respectively. Furthermore, the hot-luminescence band at 2.34 eV corresponds to the zone edge phonon at $k \sim \pi/a(0.9, 0.9, 0.9)$ with high density of states near the L-point along <111> direction.

The absorption process upon laser excitation involves interaction with a phonon, followed by intra-band relaxation of hot-carriers by phonon emission (lower *k values*); this can occur by either a 1-phonon process involving an optical phonon near the Brillouin zone center (Γ-point) with low k values, or a 2-phonon (acoustic) process with k values with opposite signs near the Brillouin zone boundaries[26]. Because the density of states of transverse acoustic (TA) phonons near the zone boundary is much higher than that of longitudinal acoustic (LA) phonons in crystalline silicon as seen in their dispersion[24], intra-band relaxation process would be dominated by 2-TA phonons. Based on the known phonon dispersion in silicon[27], the phonon-assisted hot-luminescence process has been explained in the Supplementary

Information. The broadening of the peaks with increasing energy separation from the laser excitation suggests that many other phonon relaxation pathways also start to contribute.

Our work demonstrates the unique interplay of three (quasi) particle systems; carriers, phonons and cavity plasmons, which provide an interesting test bed to study complex processes and can also lead to new properties in engineered materials not found otherwise. The ability to obtain visible light emission from silicon devices, which are compatible with lengthscales in current electronics (>20 nm), opens up new ways to integrate active Si-based photonics with other conventional functionalities. Our technique can be applied to obtain light emission from any indirect bandgap semiconductor and will be useful for the fabrication of monolithic devices utilizing optics for ultrafast data processing.

Methods

Device fabrication

Single-crystalline undoped silicon nanowires (Sigma-Aldrich) were dispersed in ethanol and transferred onto a 150 μm-thick glass substrate. A 5 nm SiO_2 interlayer was deposited by atomic layer deposition (ALD) (Cambridge Nanotech) by alternating O_3, 3-Aminopropyltriethoxysilane (APTES), and H_2O pulses at a temperature of 150 °C. A 100 nm Ag thin film was coated to form an Ω-shaped plasmonic cavity by using an e-beam evaporator at a low deposition rate of 0.2 Å/s for the first 50 nm and 0.5 Å/s for the remaining film. Ag bowtie structures were fabricated on Si substrates after etching the native oxide. The silicon substrate was covered with 5 nm SiO_2 layer grown via ALD. After the ALD process, bowties were patterned by electron-beam lithography followed by the deposition of 30 nm-thick Ag by electron-beam evaporation.

Optical measurements at room temperature

Silicon nanowires coupled with Ω-shaped plasmonic nanocavities were optically excited through the 150 μm-thick glass substrate using a home-built microscope equipped with a 60×, 0.7 NA objective (Nikon), having a spatial detection resolution of 500 nm. Planar Si with the bowtie structures was excited from the top side. A continuous wave argon-ion laser (Coherent) tuned at a wavelength of 457.9 nm was focused to pump the individual nanowires with the beam spot size of 2 μm on the sample with an excitation power of ∼250 kW/cm^2. For UV excitation, a frequency doubled femtosecond pulsed Ti:Sapphire laser (Chameleon) was tuned at a central wavelength of 355.7 nm. Photoluminescence spectra were collected using a spectrometer (Acton-SP 500i) and a cooled charge coupled device (CCD) (Pixis 2K, Princeton Instruments) with a spectral resolution of 0.5 nm.

Numerical calculation

Simulations were performed for the silicon nanowire coupled with the Ω-shaped plasmonic nanocavity structures with a pulsed point dipole source inside the cavity using a commercial finite-difference-time-domain (FDTD) software package (Lumerical). The eigenmodes, quality factors (Q), and field intensity profiles were analyzed by Fourier transforming the calculated time-domain data to the frequency-domain. By performing three-dimensional FDTD simulations, the Purcell factor, $\Gamma/\Gamma_0 = 3Q(\lambda / 2n)^3 / 2\pi V_{eff}$, was obtained by

calculating the effective mode volume (V_{eff}) where λ and n are the free space wavelength and refractive index respectively[18]. The effective mode volume of the plasmonic cavity modes can be expressed by[28]

$$V_{eff} = \frac{\int \varepsilon(r) E^2(r) d^3 r}{(\varepsilon(r) E^2(r))_{dip}}$$

where $\varepsilon(r)$ is the material dielectric constant. E_{dip} was taken in the silicon medium at the position where a dipole emitter would experience the calculated Purcell factor and the electric field intensity is integrated over the entire mode structure. The frequency-dependent real and imaginary parts of the dielectric function of Ag were obtained via an analytical fit to experimental data[29] and the real and imaginary parts of refractive indices of Si and SiO_2 were taken from ref. 30.

Quantum efficiency estimation

We first estimated the optical power collection efficiency in the optical fiber coupled spectrometer with CCD, which was used for the photoluminescence measurements. By measuring a known laser power from the integrated counts with taking into account the quantum yield and the sensitivity of the CCD, the collection efficiency was estimated to be 1%. From the integrated photon counts of the photoluminescence spectrum from the sample, the photoluminescence power through the objective was measured to be 0.8 nW. Three-dimensional FDTD calculations were carried out for Si nanowire coupled with Ω-shaped cavity (d = 70 nm, l = 8 μm) to obtain an overall far-field out-coupling efficiency of 0.059% through the entire emission spectral range after considering the numerical aperture of objective, resulting in the actual power of 1.4 μW emitted from Si. In addition, the absorption efficiency of 1% for the same plasmonic silicon with Ω-shaped cavity was calculated at the laser wavelength of 457.9 nm with a 2 μm beam size (FWHM) using the FDTD technique to fully take into account possible absorption enhancement due to the antenna effect (Supplementary Fig. S10), giving rise to the absorbed power in Si of 100 μW at the incident laser power of 10 mW. Therefore, the quantum efficiency of 1.4% was estimated by taking the ratio of the emission power from Si (1.4 μW) to the absorbed power in Si (100 μW).

Supplementary Material

Refer to Web version on PubMed Central for supplementary material.

Acknowledgments

This work was supported by the U.S. Army Research Office under Grant No. W911NF-09-1-0477 and W911NF-11-1-0024, and the National Institutes of Health through the NIH Director's New Innovator Award Program, 1-DP2-7251-01. C. O. A. is supported by the United States Department of Defense, Air Force Office of Scientific Research, National Defense Science and Engineering Graduate (NDSEG) Fellowship. We thank Akram Boukai (Michigan) and Jonathan Spanier (Drexel) for providing VLS-grown Si nanowire substrates.

References

1. Xu Q, Schmidt B, Pradhan S, Lipson M. Micrometre-scale silicon electro-optic modulator. Nature. 2005; 435:325–327. [PubMed: 15902253]
2. Liang D, Bowers JE. Recent progress in lasers on silicon. Nature Photon. 2010; 4:511–517.
3. Fan L, et al. An all-silicon passive optical diode. Science. 2012; 335:447–450. [PubMed: 22194410]
4. Cullis AG, Canham LT. Visible light emission due to quantum size effects in highly porous crystalline silicon. Nature. 1991; 353:335–338.
5. Wilson WL, Szajowski PF, Brus LE. Quantum confinement in silze-selected, surface-oxidized silicon nanocrystals. Science. 1993; 262:1242–1244. [PubMed: 17772645]
6. Brongersma ML, et al. Tuning the emission wavelength of Si nanocrystals in SiO_2 by oxidation. Appl Phys Lett. 1998; 72:2577–2579.
7. Walavalkar SS, et al. Tunable visible and near-IR emission from sub-10 nm etched single-crystal Si nanopillars. Nano Lett. 2010; 10:4423–4428. [PubMed: 20919695]
8. Park NM, Kim TS, Park SJ. Band gap engineering of amorphous silicon quantum dots for light-emitting diodes. Appl Phys Lett. 2001; 78:2575–2577.
9. Walters RJ, Bourianoff GI, Atwater HA. Field-effect electroluminescence in silicon nanocrystals. Nature Matter. 2005; 4:143–146.
10. Schmidt P, Berndt R, Vexler MI. Ultraviolet light emission from Si in a scanning tunneling microscope. Phys Rev Lett. 2007; 99:246103. [PubMed: 18233462]
11. de Boer WDAM, et al. Red spectral shift and enhanced quantum efficiency in phonon-free photoluminescence from silicon nanocrystals. Nature Nanotech. 2010; 5:878–884.
12. Goldman JR, Prybyla JA. Ultrafast dynamics of laser-excited electron distributions in silicon. Phys Rev Lett. 1994; 72:1364–1367. [PubMed: 10056694]
13. Sabbah AJ, Riffe DM. Femtosecond pump-probe reflectivity study of silicon carrier dynamics. Phys Rev B. 2002; 66:165217.
14. Prokofiev AA, et al. Direct bandgap optical transitions in Si nanocrystals. JETP Letters. 2009; 90:758–762.
15. Fujita M, Tanaka Y, Noda S. Light emission from silicon in photonic crystal nanocavity. IEEE J Sel Topics Quantum Electron. 2008; 14:1090–1097.
16. Lo Savio R, et al. Room-temperature emission at telecom wavelengths from silicon photonic crystal nanocavities. Appl Phys Lett. 2011; 98:201106.
17. Cho CH, et al. Tailoring hot-exciton emission and lifetimes in semiconducting nanowires via whispering-gallery nanocavity plasmons. Nature Mater. 2011; 10:669–675. [PubMed: 21765398]
18. Purcell EM. Spontaneous emission probabilities at radio frequencies. Phys Rev. 1946; 69:681.
19. Ryu HY, Notomi M. Enhancement of spontaneous emission from the resonant modes of a photonic crystal slab single-defect cavity. Opt Lett. 2003; 28:2390–2392. [PubMed: 14680192]
20. Baba T, Sano D. Low-threshold lasing and Purcell effect in microdisk lasers at room temperature. IEEE J Select Topics Quantum Electron. 2003; 9:1340–1346.
21. Englund D, et al. Controlling the spontaneous emission rate of single quantum dots in a two-dimensional photonic crystal. Phys Rev Lett. 2005; 95:013904. [PubMed: 16090618]
22. Barnes WL, Dereux A, Ebbesen TW. Surface plasmon subwavelength optics. Nature. 2003; 424:824–830. [PubMed: 12917696]
23. Kittel, C. Introduction to solid state physics. Wiley; 2005. p. 106-129.
24. Wei S, Chou MY. Phonon dispersion of silicon and germanium from first-principles calculations. Phys Rev B. 1994; 50:2221–2226.
25. Chelikowsky JR, Cohen ML. Electronic structure of silicon. Phys Rev B. 1974; 10:5095–5107.
26. Racek W, Bauer G, Kahlert H. Dynamic measurement of hot-electron magnetophonon effect in *n*-InSb at 11 K. Phys Rev Lett. 1973; 31:301–304.
27. Temple PA, Hathaway CE. Multiphonon Raman spectrum of silicon. Phys Rev B. 1973; 7:3685–3697.

28. Andreani LC, Panzarini G, Gérard JM. Strong-coupling regime for quantum boxes in pillar microcavities: Theory. Phys Rev B. 1999; 60:13276–13279.
29. Johnson PB, Christy RW. Optical constants of noble metals. Phys Rev B. 1972; 6:4370–4379.
30. Palik, ED. Handbook of Optical Constants of Solids. Academic; 1998.

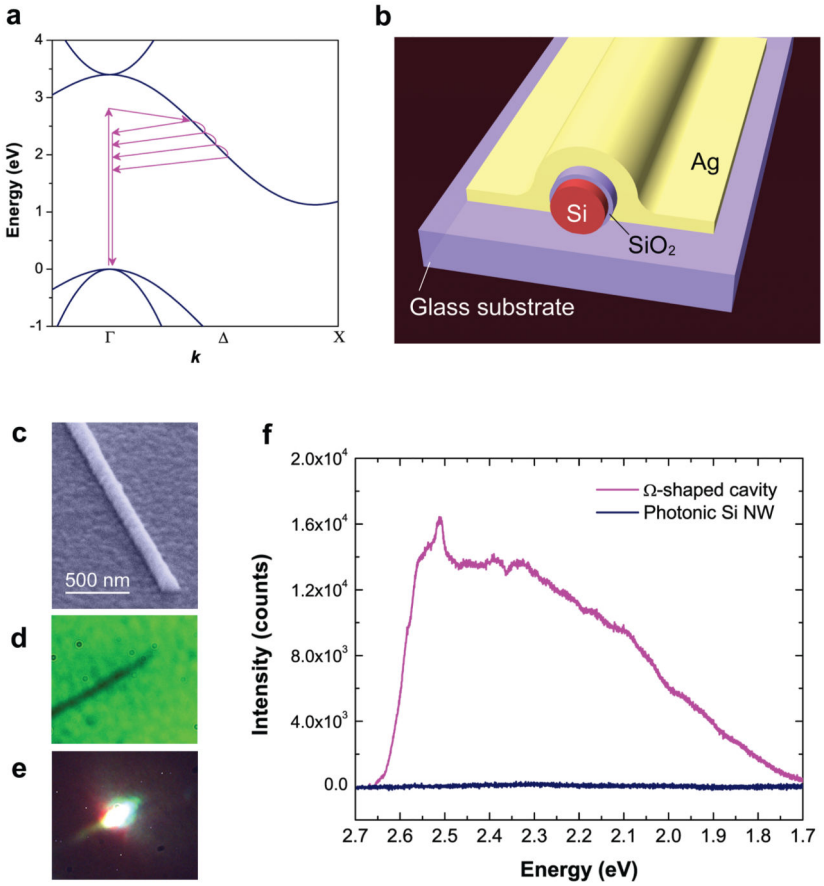

Figure 1. Hot-luminescence from silicon coupled to a plasmon nanocavity

a, Schematic of the electronic band diagram of bulk crystalline silicon illustrating phonon-assisted hot-luminescence processes before the thermalization of the carriers to the minimum of the conduction band near the X-point. **b**, Schematic of an Ω-shaped plasmonic nanocavity coupled silicon nanowire device. **c**, Scanning electron microscope (SEM) image of the fabricated device. **d and e**, Optical images of a single-plasmonic silicon nanowire device obtained through the glass substrate under white light (**d**), and a focused laser excitation (**e**). **f**, Room-temperature photoluminescence spectra from single silicon nanowire device coupled with Ω-shaped (magenta) cavity (100 nm Ag film) having the silicon nanowire diameter, *d*, of 65 nm. Spectrum of a 5 nm SiO_2 coated single silicon nanowire without a plasmonic cavity (blue; d = 60 nm) is also shown, with no observable photon counts without the plasmonic cavity.

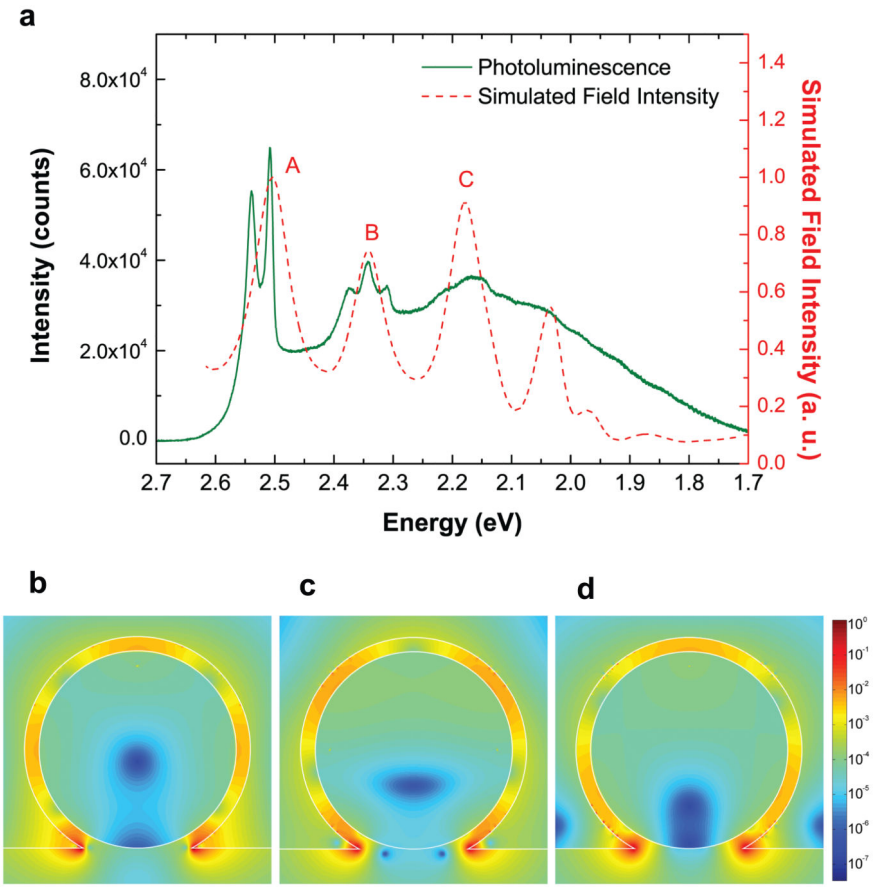

Figure 2. Resonantly enhanced hot-luminescence in plasmonic silicon

a, Room-temperature photoluminescence spectrum from a single silicon nanowire coupled with Ω-shaped plasmon nanocavity (*d* = 70 nm). The calculated frequency-dependent electromagnetic field intensity inside the cavity reproduces the resonances correctly. **b to d**, Calculated electric field profile at cavity resonance energies of 2.505 eV (**b**), 2.342 eV (**c**), and (**d**) 2.179 eV labeled as A, B, and C on the spectrum, showing the formation of plasmonic cavity modes. The corresponding magnetic field intensities of the cavity modes are provided in the Supplementary Figure S3. The white outlines refer to the Si-SiO_2-Ag interfaces of the Ω-shaped cavity structure.

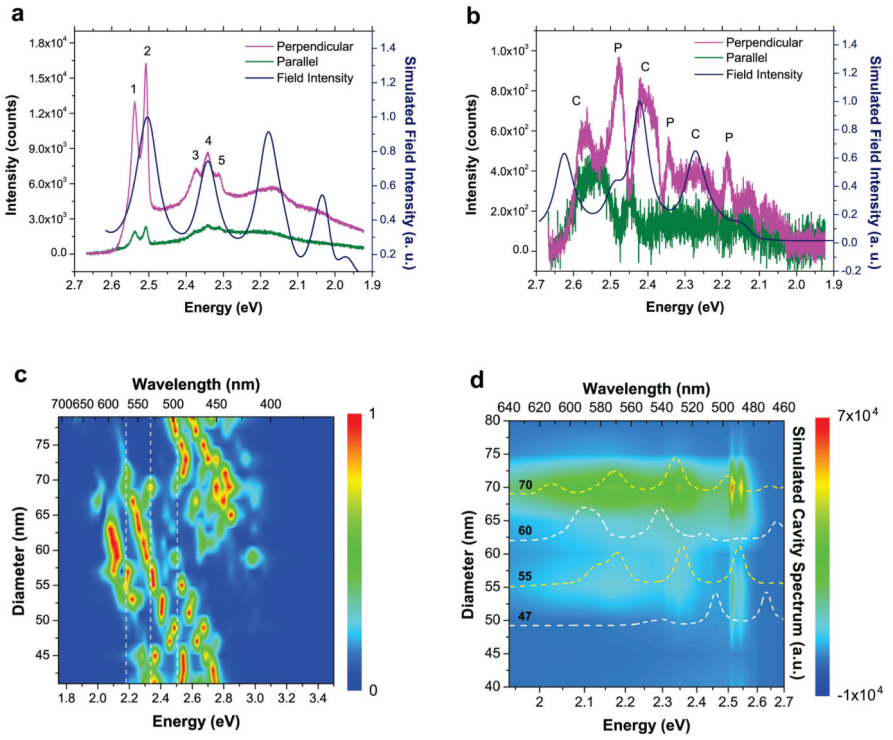

Figure 3. Polarization-selective spectra for resonant and nonresonant plasmonic silicon devices

a, Polarization-resolved hot-luminescence spectra for a resonant-sized plasmonic cavity coupled silicon nanowire (*d* = 70 nm) showing anisotropic emission polarized predominantly perpendicular to the nanowire's long axis. The strong emission bands are exactly overlapped with the calculated energy-dependent field intensity inside the cavity showing resonances. **b**, The same measurement procedure was followed for a nonresonant-sized plasmonic cavity-coupled silicon nanowire device (*d* = 50 nm). Both the cavity modes ("C") and hot-luminescence bands ("P") corresponding to phonons with high density of states are revealed on the perpendicularly polarized emission spectrum. The cavity modes are confirmed by the calculated cavity field intensity as a function of energy. **c**, Calculated field intensity spectra inside the plasmon cavities as a function of nanowire diameter. The white dashed lines indicate the three strong hot-luminescence bands, corresponding to the phonon modes with high density of states. **d**, Experimental size-dependent photoluminescence spectra for the nanowires with diameter ranging from 40 to 80 nm. Calculated spectra for cavity field intensity (dashed lines) are also plotted to show the resonant and non-resonant conditions between the cavity modes and the highly emissive hot-luminescence bands.